https://doi.org/10.1016/j.compchemeng.2020.107220

Energy system optimization model for tissue papermaking process

Yang Zhang[1], Mengna Hong[1], Jigeng Li[1], Jingzheng Ren[2], Yi Man[2,*]

1. State Key Laboratory of Pulp and Paper Engineering, South China University of Technology, Guangzhou 510640, China
2. Department of Industrial and Systems Engineering, The Hong Kong Polytechnic University, Hong Kong, China

* Corresponding author: Yi Man, Email: yi.man@polyu.edu.hk

Abstract: The drying process accounts for the largest proportion of energy consumption in paper mills. Energy system optimization has a great significance for reducing the energy consumption of the paper drying process. The drying process is a complex system that consists of several subsystems, such as cylinder and air hood systems. Previous optimization models for energy systems usually focused on these subsystems. A global optimization methodology for the entire drying process is lacking, and no existing models can be applied in practice. In this work, an energy system optimization model for the tissue paper drying process is proposed based on a process simulation model. The modeling process integrates the various subsystems and fully considers the coupling of the paper drying process, which greatly enhances the industrial application value of the model. Industrial operating data are used to test the simulation model, and the results show that the simulation error of each key variable is within 5%, which meets the real-world production requirements and lays the foundation for an energy efficiency analysis of each subsystem. Applying the optimization model to a tissue paper mill, the results show that it can reduce drying costs by 8.71%.

Keywords: Tissue paper; Drying process; Process simulation; Energy system optimization

1. Introduction

The papermaking industry is the fourth largest energy-intensive industry (Man et al. 2019a). It accounts for approximately 7% of the global industrial energy consumption (Hu et al. 2019). As a major papermaking country, China consumes approximately 1.5×10^6 GJ of energy every year for the production of pulp and paper products (Lin and Zheng 2017). Although the average energy consumption for one ton of paper product has decreased from 45 MJ (2000) to 33 MJ (2015), there is still a potential for saving 15–45% of the energy currently used (Peng et al. 2015). According to the *Paris Climate Agreement*, China is obliged to lower its gross domestic production (GDP) of CO_2 by 60–65% of the 2005 level and increase the proportion of non-fossil fuels in its total energy to approximately 20% by 2030 (Nouri et al. 2018). Energy saving and emission reduction have become the most important and urgent tasks in China's papermaking industry, and their success may enable China to fulfill the goals of the *Paris Climate Agreement* (Man et al. 2019b).

Tissue paper is one of the most important paper product types. Being a daily necessity, the consumption growth of tissue paper is much higher than that of other paper products. From 2010 to 2019, the average annual growth rate of tissue paper production was 5.51%, which was significantly higher than the overall level of 1.28%. However, there is still a large difference in tissue paper consumption between China and other developed countries; in 2017, tissue paper consumption in China was 6.1 kg per capita while it was 16 kg per capita in Japan and 22 kg per capita in the US. The tissue paper industry in China still has great development potential.

Despite the broad market prospects, tissue paper mills are facing urgent issues regarding energy saving and emission reduction due to the strict environmental protection requirements of the government (Chen et al. 2018). Research on energy saving and consumption reduction is of great significance for improving the competitiveness of tissue paper making enterprises and reducing the energy consumption of the papermaking industry.

Dewatering is the most important part of the papermaking process (Chen et al. 2016). To meet the required strength and quality standards, the dryness of the finished tissue

paper is usually controlled at 92–95%. In all papermaking dewatering processes, the drying process has the highest energy consumption and accounts for approximately 70% of the total energy consumption of the papermaking process (Man et al. 2017). Reducing the energy consumption of the drying process is the key to a green and sustainable papermaking process.

The proper adjustment of the operating parameters has a great impact on the energy consumption of the paper drying process, and an effective optimization method depends on the accurate monitoring of the key variables of the drying process (Geng et al. 2017). Unfortunately, current paper machine control systems cannot monitor all key variables, such as paper temperature, hot air humidity, and exhaust air humidity. There are two major reasons for this: (1) The drying of paper is a continuous high-speed process in a high-temperature and high-humidity environment. The expensive sensors are easily damaged under such a drastic environment. (2) To ensure the drying effect and reduce energy consumption, the drying process is usually designed as a highly integrated system. For example, the average distance between the cylinder and the air hood is only 2–3 cm, which leaves no space for the installation of dryness and temperature sensors. In real-world production, engineers can only rely on their experience and feedback of product quality results to control and optimize the energy system of the drying process. Without the guidance of scientific calculations, the energy system cannot be operated under optimal conditions, which increases the energy consumption and production cost (Fuentes et al. 2015).

Simulation and energy system optimization models can realize the accurate monitoring of key variables and reduce the energy consumption of the drying process. In recent years, some progress has been made in these areas. Li et al. (2011) proposed a mathematical model based on the energy flow of the drying process and optimized the energy systems of newsprint and linerboard paper machines using nonlinear programming methods. Kong et al. (Kong and Liu 2012) used the cylinder group as the minimum modeling unit and the sequential module method to establish a static energy model. Ghodbanan et al. (Ghodbanan et al. 2017; 2015) simulated the drying process of fluting paper and optimized the operating parameters, such as paper dryness and

exhaust air humidity based on a nonlinear programming method. Anders et al. (Ottosson et al. 2017) proposed a paper drying process model that can predict the evaporation load of the drying process under different yields. Based on mass and energy conservation principles and heat and mass transfer mechanisms, the researchers simulated and optimized the drying process of different types of paper machines. These explorations have improved the understanding of the paper drying process and reduced energy consumption.

However, the existing simulation and energy system optimization models still have the following shortcomings: (1) The input parameters of the simulation models, such as the hot air humidity and surface temperature of the cylinders, are difficult to measure and control online. The modeling process is based on a certain subsystem of the drying process and ignores the interaction between the environment, cylinder, air hood, and paper, resulting in inaccurate model boundary conditions and limited simulation accuracy. (2) Most of the energy system optimization models are only used to optimize a single variable, such as the hot air temperature or cylinder pressure. These models do not consider changes in other process variables after optimization, such as the dew point temperature and paper dryness. (3) The Yankee cylinder occupies an absolute dominant position among tissue paper drying equipment. However, most studies focus on the drying process of a multi-cylinder, and the Yankee cylinder is rarely involved.

To solve the above problems, this paper proposes a novel modeling method for simulation and energy system optimization for the tissue paper drying process. The simulation model systematically solves the interaction between the environment, cylinder, air hood, and paper. The easily accessed and controllable variables are used as the model input to broaden its industrial application range. The energy system optimization model comprehensively considers the relationships between the dew point temperature, paper dryness, and operating parameters. In this work, two optimization algorithms are used to solve the model. One is an optimization algorithm based on energy efficiency analysis; the other is a sequential quadratic programming (SQP) method for solving nonlinear programming problems.

2. Methods and data

Drying is a key process in reducing the energy consumption of papermaking. In contrast to the previous optimization models for the energy system, the model proposed in this work comprehensively considers the coupling between all subsystems and establishes an energy system optimization model based on accurate simulation of the key variables.

2.1. Drying process of tissue paper

The drying process of tissue paper is shown in Fig. 1. The wet paper is transferred to the Yankee cylinder through the press roll and passed through four drying zones: *ab, bc, cd*, and *de* on the cylinder. Point *a* is the position where the paper is separated from the press roll and attached to the surface of the cylinder; point *b* is the position where the paper enters the wet side air hood; point *c* is the position where the paper enters the dry side air hood; point *d* is the position where the paper leaves the air hood; and point *e* is the position where the paper is scraped away from the cylinder by the wrinkle scraper. The paper is heated by two hot streams in zones *bc* and *cd*: heat transfer in contact with the cylinder, and convective heat transfer with the high-speed airflow of the air hood. Therefore, the evaporation of paper moisture in these two drying zones is much greater than in the *ab* and *ed* zones.

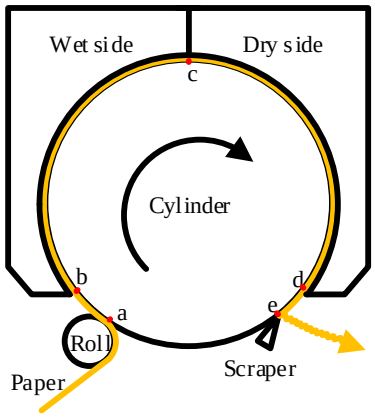

Fig. 1. Schematic diagram of Yankee cylinder system

The air hood system of the drying process is shown in Fig. 2. After the fresh air is heated, it is blown from the nozzles of the air hood panel onto the paper. The humid air containing a large amount of evaporated moisture is discharged from the air hood

exhaust pipeline and is divided into two parts: one part is discharged by the exhaust fan and is no longer used, and the other part is mixed with fresh air and then sent to the air hood again after being heated. In this way, the air circulates continuously in the pipeline. In Fig. 2, 1 and 9 represent the hot air sent to the wet and dry side air hood, respectively; 2 and 10 represent the suction air through the wet and dry side gaps of the air hood, respectively; 3 and 11 represent the evaporated water vapor of the wet and dry side air hoods, respectively; 4 and 12 represent the exhaust air of the wet and dry side air hood, respectively; 5 and 13 represent the parts that are no longer used in the exhaust air of the wet and dry side air hood, respectively; 6 and 14 represent the reused air of the wet and dry side air hood, respectively; 7 and 15 represent the fresh air of the wet and dry side air hood, respectively; 8 and 16 represent the mixed air of the wet and dry side air hood, respectively; and 17 represents the total fresh air.

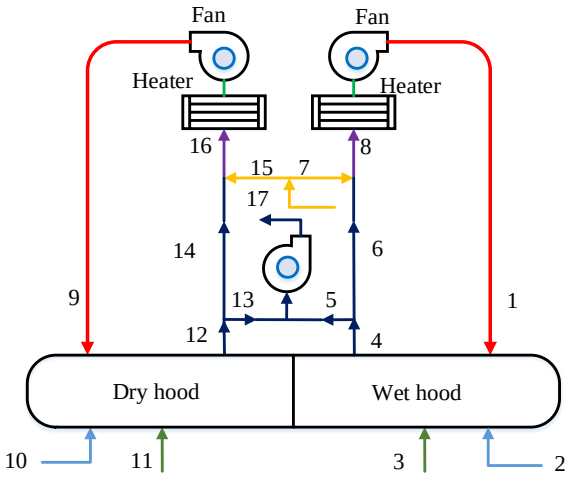

Fig. 2. Schematic diagram of the air hood

The data used for modeling in this work are collected from the production process of a tissue paper mill. The collected data are divided into three parts, namely, the geometric and historical operating parameters of the paper machine and the paper drying process parameters that can be regarded as constants. These data are described in detail in Appendix A.

The historical operating data of the drying process include the hot air temperature, fan frequency, cylinder pressure, production speed, paper weight, and coiling rate. The input of the paper drying process simulation model also includes the ambient temperature and humidity. The processed historical operating data are shown in Appendix B.

2.2. Modeling route

In tissue paper production, paper drying is a very complex process, mainly reflected in that it involves a variety of materials (paper, hot air, water vapor, steam) and multiple processes (heat and mass transfer), which are jointly determined by the drying energy system and production raw materials. Therefore, a decoupling strategy needs to be found to clearly characterize the joint drying effect of hot air (air hood) and steam (cylinder) on the paper, as well as the joint influence of water vapor (paper) and ambient air on the hot air state of the air hood. This work establishes three different models for decoupling. The overall technical route of this work is shown in Fig. 3, which mainly includes the establishment process of the paper drying process simulation and energy system optimization models. The paper drying process simulation model includes three parts: the air hood, paper drying, and energy consumption models. First, the air hood model is established to simulate the air state at each point of the air hood during stable production. It includes environmental parameters, paper parameters, production parameters (such as production speed) and operating parameters of the air hood system. Then, a paper drying model is established to simulate the temperature and humidity of paper, which includes the paper parameters, the output of the air hood model, production parameters, the operating parameters of the air hood system and the cylinder system, and the paper machine parameters. During the simulation, the cylinder is divided into multiple sections with lengths of 1 mm along the circumferential direction, and the paper drying model is used to gradually solve the temperature and humidity, and heat transfer of paper in each section. Finally, based on the air hood model and the paper drying model, an energy consumption model is established to simulate the energy consumption of the air hood system and the dryer system. Appendix C shows the transmission information of the main parameters in the simulation model. To scientifically formulate optimization strategies, the paper drying process simulation model is used to analyze the drying cost and energy efficiency of the drying process. Based on the analysis results, the energy system optimization model is established, and an algorithm for solving the model is designed. This work also uses SQP to solve the optimization model as a comparison.

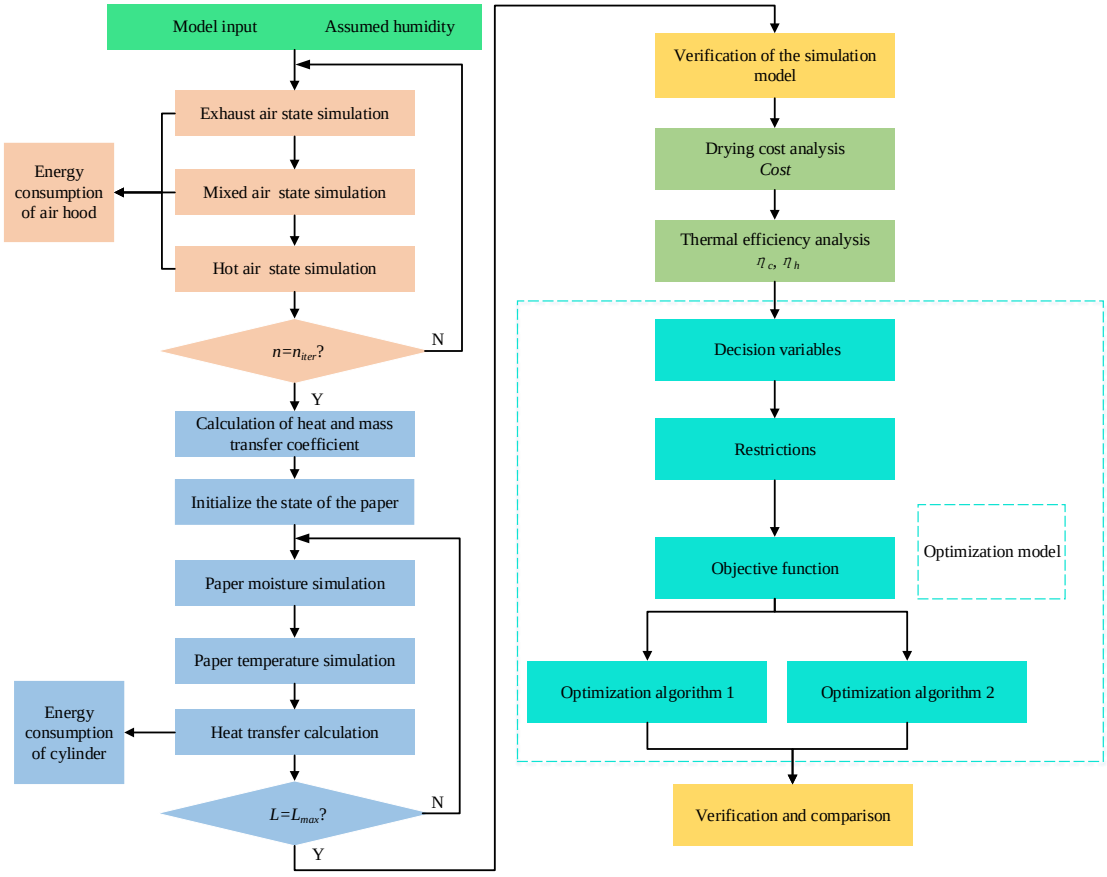

Fig. 3. Overall technical route of the modeling process

2.3. Simulation model for the key process of energy saving

2.3.1. Air hood

The water vapor pressure difference between the surface of paper and air determines the levels of evaporation and mass transfer (Chen et al. 2019). Therefore, the hot air humidity determines the drying effect of the paper. Previous studies usually took this variable as a constant, and did not establish relevant models to simulate it, which led to huge simulation deviations. As shown in the Fig. 2, the hot air (1 or 9) status is affected by the air status of other points in the air hood, that is, the hot air status of these points is coupled. How to decouple and solve the hot air humidity when the paper machine runs stably is a problem to be solved. Based on the law of conservation of mass and energy, this work proposed an iterative solution method to simulate the hot air humidity of the paper machine in stable operation under a set of operating parameters (production speed, paper weight, fan frequency, hot air temperature, etc.),

so as to simulate the steam pressure difference between the air and the paper surface.

Because the structure of the wet side air hood is the same as that of the dry side air hood, the wet side air hood is taken as an example to derive the modeling process. An analysis of the paper machine from the start to the stable process shows that if the operating parameters are determined, regardless of the initial state of the air hood, it will eventually reach a stable state. The temperature, humidity, density, and mass flow of each point in the pipeline influence each other. In this work, the air hood model is established to simulate the air state in the pipeline during the stable operation of the paper machine. The calculation formulae for the density and enthalpy of the humid air required in the modeling process are shown in equations (1)–(3) (Heikkilä and Milosavljevic 2003; Lu and Shen 2007).

$$P_a = \frac{P_{tot}X}{X+0.622} \tag{1}$$

$$\rho = \frac{0.0034843(P_a - 0.3779P_{tot})}{T+273.15} \tag{2}$$

$$H = 10^3[1.01T + (2501 + 1.85T)X] \tag{3}$$

where P_{tot} and P_a represent the total air pressure and water vapor partial pressure, respectively (Pa); X represents the air humidity (kg water/kg dry air); ρ represents the air density (kg/m^3); T represents the air temperature (℃); and H represents the enthalpy of air (J/kg dry air).

When the paper machine is turned on, the moisture content of the hot air is the same as the moisture content of the air in the workshop, as shown in equation (4):

$$X_1^{(1)} = X_7 \tag{4}$$

where $X_1^{(1)}$ represents the humidity of the hot air at the first iteration (kg water/kg dry air), and X_7 represents the air humidity of the environment (kg water/kg dry air). X_7 is not affected by the air hood and does not participate in the iteration process.

The temperature, humidity, and mass flow of the exhaust air are determined by the hot air, suction air, and evaporation of the paper moisture. The mass of dry air and water in and out of the air hood are conserved, and the total energy is also conserved, as shown in equations (5)–(7):

$$\frac{q_{m4}^{(1)}}{1+X_4^{(1)}} = \frac{q_{m1}^{(1)}}{1+X_1^{(1)}} + \frac{q_{m2}^{(1)}}{1+X_2} \tag{5}$$

$$\frac{q_{m4}^{(1)}X_4^{(1)}}{1+X_4^{(1)}} = \frac{q_{m1}^{(1)}X_1^{(1)}}{1+X_1^{(1)}} + \frac{q_{m2}^{(1)}X_2}{1+X_2} + q_{m3} \tag{6}$$

$$\frac{q_{m4}^{(1)}H_4^{(1)}}{1+X_4^{(1)}} = \frac{q_{m1}^{(1)}H_1^{(1)}}{1+X_1^{(1)}} + \frac{q_{m2}^{(1)}H_2}{1+X_2} + q_{m3}H_3 \tag{7}$$

where q_m represents the air mass flow (kg/s).

The air hood balance rate is defined as the ratio of dry air mass flow in and out of the air hood, which can be determined by manually measuring the air flow of the pipeline. In this work, HB is used to calculate the suction air mass flow, as shown in equation (8):

$$HB = \frac{q_{m1}^{(1)}}{1+X_1^{(1)}} / \frac{q_{m4}^{(1)}}{1+X_4^{(1)}} \tag{8}$$

where X_2 represents the moisture content of the suction air, which is the same as the moisture content of the workshop air.

The dry air mass of the air hood is conserved, as shown in equation (9).

$$\frac{q_{m5}^{(1)}}{1+X_5^{(1)}} = \frac{q_{m7}^{(1)}}{1+X_7^{(1)}} + \frac{q_{m2}^{(1)}}{1+X_2} \tag{9}$$

The mass of dry air and water in the air hood are conserved, and the total energy of the material is also conserved, as shown in equations (10)–(12).

$$\frac{q_{m8}^{(1)}}{1+X_8^{(1)}} + \frac{q_{m5}^{(1)}}{1+X_5^{(1)}} = \frac{q_{m4}^{(1)}}{1+X_4^{(1)}} + \frac{q_{m7}^{(1)}}{1+X_7^{(1)}} \tag{10}$$

$$\frac{q_{m8}^{(1)}X_8^{(1)}}{1+X_8^{(1)}} + \frac{q_{m5}^{(1)}X_5^{(1)}}{1+X_5^{(1)}} = \frac{q_{m4}^{(1)}X_4^{(1)}}{1+X_4^{(1)}} + \frac{q_{m7}^{(1)}X_7^{(1)}}{1+X_7^{(1)}} \tag{11}$$

$$\frac{q_{m8}^{(1)}H_8^{(1)}}{1+X_8^{(1)}} + \frac{q_{m5}^{(1)}H_5^{(1)}}{1+X_5^{(1)}} = \frac{q_{m4}^{(1)}H_4^{(1)}}{1+X_4^{(1)}} + \frac{q_{m7}^{(1)}H_7^{(1)}}{1+X_7^{(1)}} \tag{12}$$

The humidity remains unchanged before and after heating, as shown in equation (13).

$$X_1^{(2)} = X_8^{(1)} \tag{13}$$

When the paper machine runs stably, the temperature, humidity, mass flow, enthalpy, and density of air no longer change. After several iterations according to the calculation process of equations (4)–(13), the stable hot air humidity can be obtained. The determination method and results of the maximum iteration number n_{iter} of the air hood model are described in detail in Appendix D.

2.3.2. Paper drying

Compared with the multi-cylinder drying energy system, the air hood has a greater influence on the drying process of tissue paper. The coupling between heat transfer and mass transfer is stronger because the hot air has a high velocity after being ejected through the air hood nozzles. In this work, a decoupling method of solving the heat transfer coefficient first and then the mass transfer coefficient is adopted, and the solution methods of the heat transfer coefficient and mass transfer coefficient outside and inside the air hood are designed respectively, which made the simulation more accurate. The heat transferred to the paper by the cylinder and air hood is used to evaporate the water in the paper, overcome the capillary adsorption, and increase the paper temperature. The paper temperature and humidity are coupled with each other. According to the paper drying kinetic model, the rate of change of the humidity X_p and temperature T_p of the paper are shown in equations (14)–(15) (Ortega and Juan Rosales 2018; Welty et al. 1976; Gonor 2002; Katsiampoura et al. 2018).

$$\frac{dX_p}{dt} = -\frac{K_m}{G} \cdot \frac{M_w P_{tot}}{R(T_p+273.15)} ln(\frac{P_{tot}-P_a}{P_{tot}-P_p}) \tag{14}$$

$$\frac{dT_p}{dt} = \frac{h_{s-p}(T_s-T_p)+h_{ap}(T_a-T_p)+G(\Delta H_v+\Delta H_s-C_{pw}T_p)\frac{dX_p}{dt}}{G(C_{pf}+X_p C_{pw})} \tag{15}$$

where X_p represents the paper humidity (kg water/kg absolute dry fiber); T_p represents the paper temperature (℃); t represents the drying time (s); K_m represents the convective mass transfer coefficient between the paper and air (m/s); G represents the absolute dry weight of paper (kg/m^2); R represents the ideal gas constant (J/(mol·K)); P_p represents the partial pressure of water vapor on the paper surface (Pa); M_w represents the molar mass of water (kg/mol); h_{s-p} represents the total heat transfer coefficient from the steam in the cylinder to the paper (W/(m^2·℃)); h_{ap} represents the convective heat transfer coefficient between the paper and air (W/(m^2·℃)); T_s represents the steam temperature in the cylinder (℃); T_a represents the air temperature on the surface of the paper (℃); C_{pf} and C_{pw} represent the specific heat of the fiber and water, respectively (kJ/(kg·℃)); ΔH_v represents the enthalpy change in the water vapor vaporized from the paper (J/kg). ΔH_s represents

the adsorption heat of the water in the paper (J/kg), which is determined by the temperature and the humidity of paper, and it is calculated as shown in equations (16)–(17):

$$\Delta H_s = 0.10085R\frac{1-\varphi}{M_w\varphi}{X_p}^{1.0585}(T_p + 273.15)^2 \tag{16}$$

$$\varphi = 1 - exp\,(-47.58{X_p}^{1.87} - 0.10085T_p{X_p}^{1.0585}) \tag{17}$$

where φ represents the relative humidity of the air on the surface of paper.

To solve the humidity and temperature of the paper in different drying areas, $\frac{\mathrm{d}L}{v}$ is used instead of dt in equations (14)–(15). The humidity and temperature distribution equations of the paper are obtained, as shown in equations (18)–(19) (Erkkila et al. 2015; Di Marco et al. 2016):

$$\frac{dX_p}{dL} = -\frac{K_m}{Gv}\cdot\frac{M_wP_{tot}}{R(T_p+273.15)}ln(\frac{P_{tot}-P_a}{P_{tot}-P_p}) \tag{18}$$

$$\frac{dT_p}{dL} = \frac{h_{s-p}(T_s-T_p)+h_{ap}(T_a-T_p)+G(\Delta H_v+\Delta H_s-C_{pw}T_p)\frac{dX_p}{dt}}{Gv(C_{pf}+X_pC_{pw})} \tag{19}$$

where L represents the drying distance of the paper in the circumferential direction of the cylinder (m) and v represents the production speed (m/s).

To calculate h_{s-p}, the thermal resistance is divided into two parts, namely, the thermal resistance inside the cylinder h_{sc} and the contact thermal resistance between the cylinder and paper h_{cont}, as shown in equation (20). h_{cont} is linearly related to the humidity of the paper (Lu and Shen 2007), as shown in equation (21). For a paper machine, h_{s-p} can be regarded as a constant. The determination method and results of h_{s-p} are described in detail in Appendix D.

$$\frac{1}{h_{s-p}} = \frac{1}{h_{sc}} + \frac{1}{h_{cont}} \tag{20}$$

$$h_{cont} = \alpha X_p + \beta \tag{21}$$

The convective heat transfer process between the air and paper is similar to the air flow across a flat plate. In the *ab* and *de* sections of the drying zone, h_{ap} can be obtained by equation (22) (Grimm et al. 2019). The mass transfer rate in the drying zones of *bc* and *cd* is high, which affects the heat transfer. Therefore, the heat transfer coefficient needs to be corrected, and the calculation of the correction factor is shown in equations (23)–(24) (Ottosson et al. 2017):

$$h_{ap0} = \frac{Nu \times \lambda_H}{L_{conv}} \tag{22}$$

$$h_{ap1} = h_{ap0} \frac{E}{e^E - 1} \tag{23}$$

$$E = -\frac{G \cdot vdX_p}{dL} \frac{C_v}{h_{ap0}} \tag{24}$$

where Nu represents the Nusselt number; λ_H represents the air thermal conductivity (W/(m·k)); L_{conv} represents the characteristic length of the convection heat transfer on the surface of the paper, taking half the distance between the paper and the nozzle, in m; and C_{v} represents the specific heat of water vapor (kJ / (kg·℃)).

The calculation method for the Nusselt number is different in different situations. In the *ab* and *de* sections of the drying zone, the standard form of the Nusselt number is used for calculation, as shown in equation (25) (Ottosson et al. 2017). In the *bc* and *cd* sections of the drying zone, its calculation method is shown in equation (26) (Soto-Meca et al. 2016):

$$Nu_{out} = \frac{0.037 Re^{0.81} Pr}{1 + 2.443 Re^{-0.1} (Pr^{\frac{2}{3}} - 1)} \tag{25}$$

$$Nu_{in} = \frac{f'^{0.9505} \left[3.649 - \frac{(0.03455 + 4.812 f')h}{d'}\right]}{1 + 60.47 f'} \times \left[0.90 + \frac{0.10}{1 + 0.056939 (T_a / 100℃)^3}\right] Re^{0.772} Pr^{1/3} \tag{26}$$

where f' represents the corrected hood nozzle opening ratio; h represents the distance from the nozzle to the paper (m); d' represents the corrected nozzle diameter (m); Re represents the Reynolds number; and Pr represents the Prandtl number.

The analog method for calculating the mass transfer coefficient based on the heat transfer coefficient is widely used in paper drying, as shown in equations (27)–(28) (Nilsson 2004):

$$K_m = \frac{h_{pa}}{\rho_a C_a} Le^{-2/3} \tag{27}$$

$$Le = \frac{\lambda_a}{\rho_a C_a D_{wa}} \tag{28}$$

where ρ_a represents the air density (kg/m^3); C_a is the air specific heat (J/(kg·℃)); λ_{a}

represents the thermal conductivity of air (W/(m·℃)); Le represents the Lewis number; and D_{wa} represents the diffusion coefficient of water vapor in the air (m^2/s). The calculation formula for D_{wa} is shown in equation (29):

$$D_{wa} = 1.87 \times 10^{-10} \frac{(T_f+273.15)^{2.072}}{9.872\times10^{-6}P_{tot}} \quad (29)$$

where T_f represents the air temperature of the boundary layer (℃), for which the commonly used calculation method is to take the average value of the paper temperature and the hot air temperature (Karalashvili et al. 2015). The air thermal physical properties, such as viscosity, thermal conductivity, specific heat, and Prandtl number, involved in the above process are all determined by the temperature and humidity of the air. For the calculation, refer to the calculation method proposed by Anders and Stefan et al. (Ottosson et al. 2017; Di Marco et al. 2016).

2.3.3. Energy consumption

The heat consumption of the cylinder is divided into three parts: the heat transferred to the paper by the cylinder outside the press area, the heat transferred to the paper in the press area and the heat loss of the cylinder, as shown in equation (30):

$$\int_0^{L_{ae}} h_{s-p}(T_s - T_P)WdL + Q_{roll} + (T_s - T_{env})\sum A_{ci}h_{ci} = \Delta H_c q_{mc} \quad (30)$$

where L_{ae} represents the total length of the drying zone along the circumference of the cylinder (m); W represents the width of paper (m); T_{env} represents the environmental temperature (℃). A_{ci} and h_{ci} represent the heat transfer coefficient and area of the *i-th* block on the cylinder shell not covered by paper, respectively. $\sum A_{ci}h_{ci}$ can be regarded as the heat loss coefficient of the cylinder (W/ ℃), and its determination method and result are described in detail in Appendix D. ΔH_c represents the enthalpy change from steam to condensate in the cylinder (J/kg); q_{mc} represents the steam flow consumed by the cylinder (kg/s); and Q_{roll} represents the heat transfer rate of the cylinder to paper in the press area (W).

Because the contact surface at the press area is extremely small, and the heat transfer coefficient of felt is difficult to determine, it is assumed that all the heat

transferred is used to heat the paper. Thus, the simplified calculation of Q_{roll} is shown in equation (31):

$$Q_{roll} = vWG(T_a - T_0)(C_{pf} + u_a C_{pw}) \tag{31}$$

where T_0 represents the temperature of the paper before it is attached to the cylinder (°C); T_a represents the temperature of the paper after pressing (°C); and u_a represents the humidity of the paper after pressing (kg water/kg dry fiber).

The energy consumption of the air hood includes the energy consumed through the heating of the air and the heat dissipating to the environment, as shown in equation (32):

$$\frac{\dot{m}_1(H_1 - H_8)}{1+X_1} + (T_1 - T_{env})\sum A_{hi}h_{hi} = \Delta H_h q_{mh} \tag{32}$$

where ΔH_h represents the enthalpy change in the steam in the air hood (J/kg); q_{mh} represents the steam flow consumed by the air hood (kg/s); T_1 represents the temperature of the hot air (°C); and $\sum A_{hi}h_{hi}$ represents the heat loss coefficient of the air hood (W/°C); its determination method and result are described in detail in Appendix D.

2.3.4. Model verification

Eighty percent of the historical operating data are used to determine the values of the three parameters: h_{s-p}, $\sum A_{ci}h_{ci}$, and $\sum A_{hi}h_{hi}$. The remaining data are used to verify the paper drying process simulation model. The key variables that need to be verified include the evaporation rate, temperature, and humidity of the exhaust air, and the steam flow of the air hood and cylinder. This work uses the mean absolute percent error (MAPE) as the model error indicator. The calculation of the MAPE is shown in equation (33) (Du et al. 2017):

$$MAPE = \frac{1}{n}\sum_{i=1}^{n}\left|\frac{\hat{y}_i - y_i}{y_i}\right| \times 100\% \tag{33}$$

where n represents the number of samples, y_i represents the actual value, and $\hat{y}_i$ represents the simulated value.

The evaporation rate is used to verify the simulation effect of the model on the

humidity of the paper, and the calculation is shown in equation (34):

$$R = \frac{(X_a - X_e)G \cdot v}{3600 L_{ae}} \tag{34}$$

where R represents the evaporation rate (kg/(m^2·h)); and X_a and X_e represent the humidity of the starting and ending points of paper on the cylinder, respectively (kg water/kg absolute dry fiber). The *MAPE* of the evaporation rate is 1.23%, and the comparison between the simulated and actual values is shown in Fig. 4.

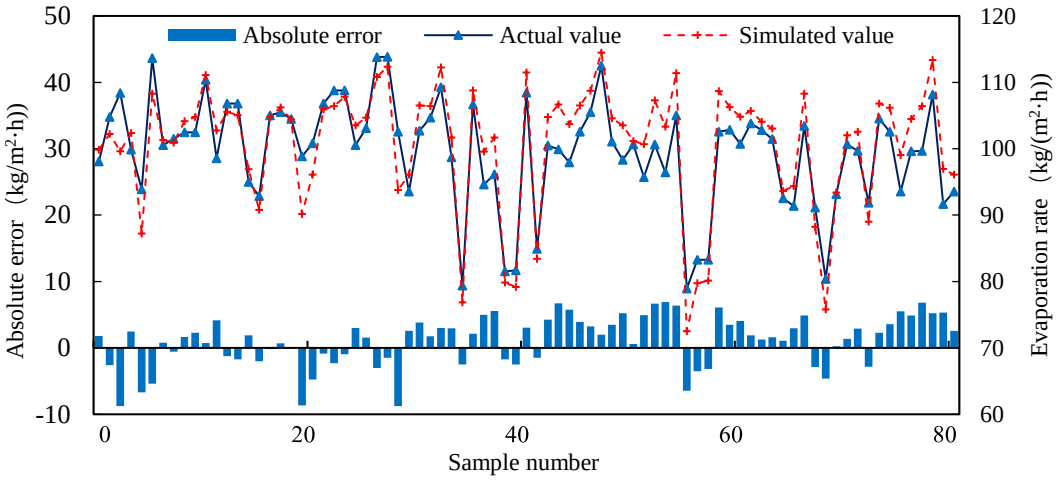

Fig. 4. Comparison of actual and simulated values of the evaporation rate

The comparison between the simulated and actual values of the exhaust air humidity on the wet and dry sides are shown in Fig. 5 and Fig. 6, respectively. The *MAPE* values for the exhaust humidity on the wet and dry sides are 2.37% and 2.27%, respectively.

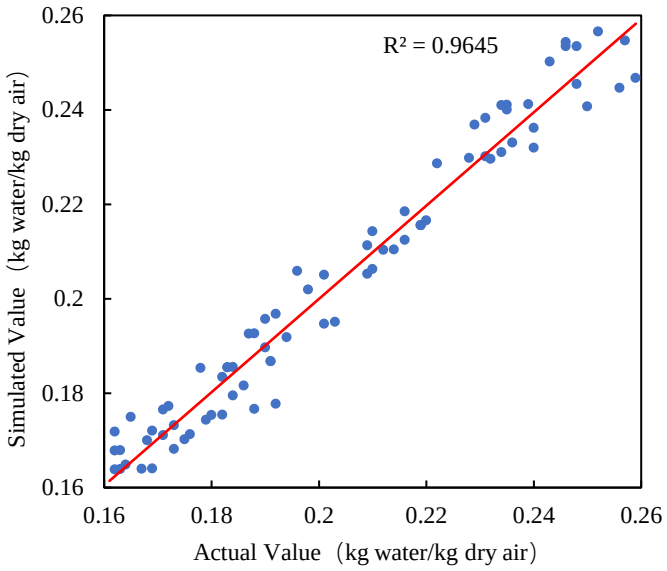

Fig. 5. Comparison of actual and simulated values of the wet side exhaust air humidity

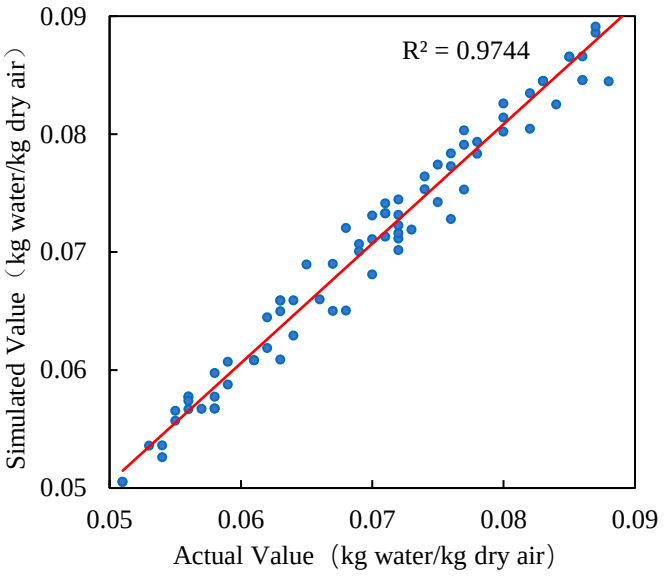

Fig. 6. Comparison of actual and simulated values of the dry side exhaust air humidity

Comparisons between the simulated and actual values of the exhaust air temperature of the air hood on the wet and dry sides are shown in Fig. 7 and Fig. 8, respectively. The *MAPE* values of the exhaust air temperature of the wet and dry sides are 4.89% and 3.78%, respectively.

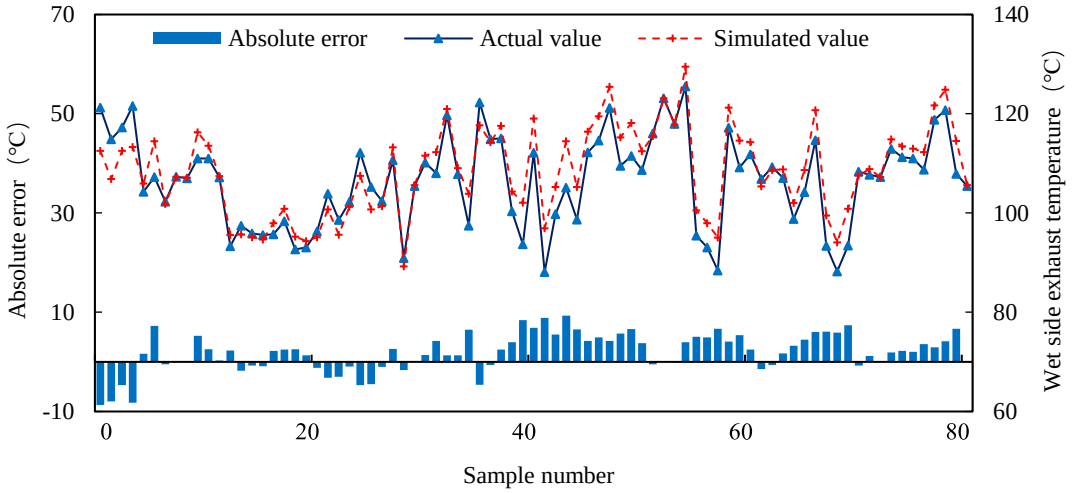

Fig. 7. Comparison of simulated and actual values of the wet side air hood exhaust air temperature

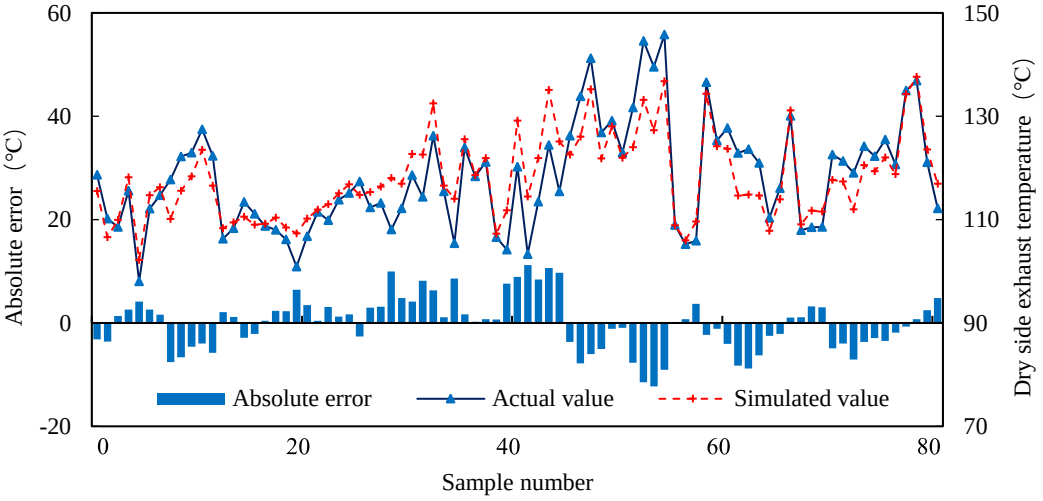

Fig. 8. Comparison of simulated and actual values of the dry side air hood exhaust air temperature

Comparisons of the simulated and actual values of the steam flow of the air hood and cylinder are shown in Fig. 9 and Fig. 10, respectively. The *MAPE* values of the steam flow simulation of the cylinder and air hood are 3.34% and 4.51%, respectively. The accurate simulation of steam flow lays the foundation for an energy efficiency analysis of the drying process. Exhaust air temperature, humidity and steam flow are the most important parameters for engineers in production. The paper drying process simulation model established in this work realizes accurate simulation of these

parameters, which can replace the role of hardware measurement.

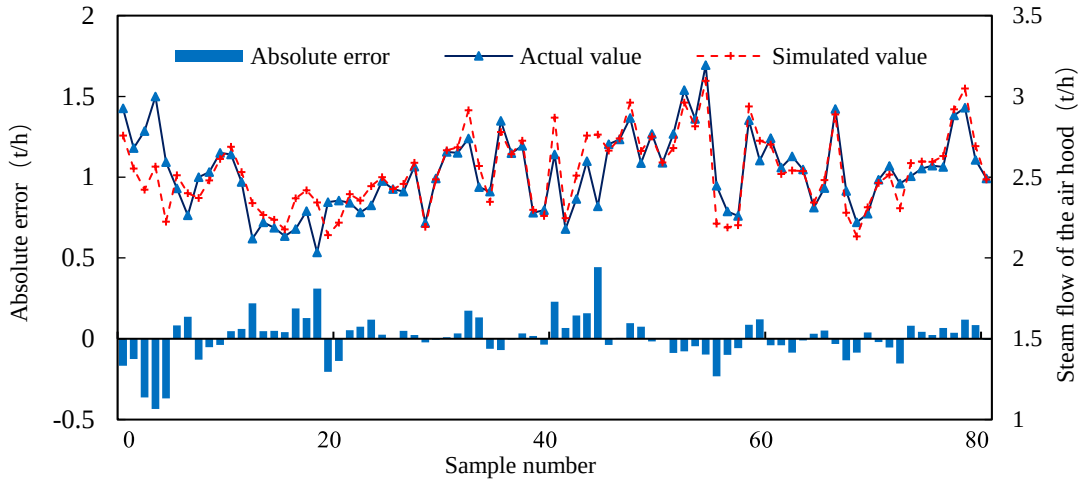

Fig. 9. Comparison of simulated and actual values of the steam flow consumed by the air hood

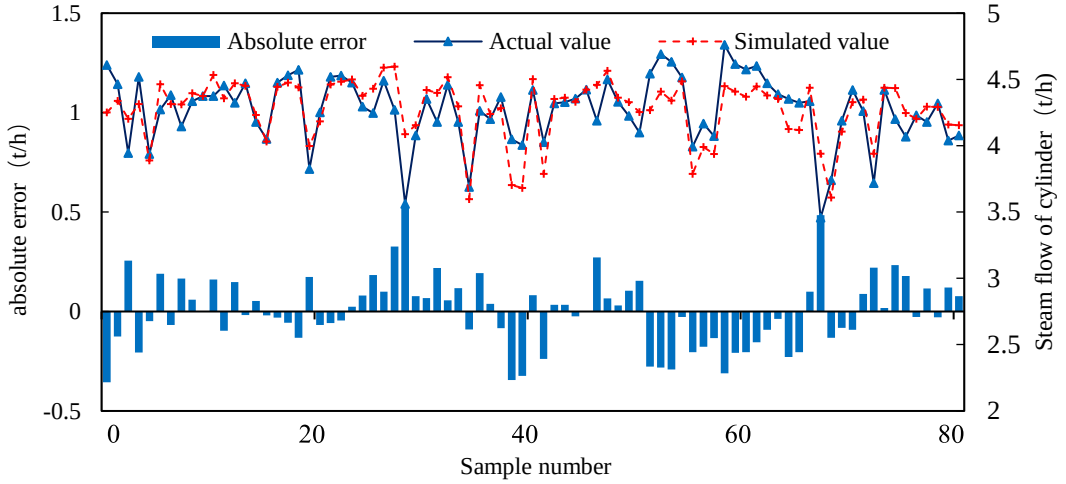

Fig. 10. Comparison of simulated and actual values of the steam flow consumed by cylinder

3. Optimization model for the key process of energy saving

Establishing an energy system optimization model is an effective way to reduce the energy consumption of the paper drying process. Previous works usually modeled subsystems, such as the cylinder system or the air hood system and could only achieve the optimization of individual operating parameters. Such models ignore the coupling between different subsystems, and the optimization results cannot be applied to actual

production. The optimization model proposed in this work is based on the accurate simulation of all key variables by the simulation model, which means that the optimization process of the model is more comprehensive and the optimization results are more reliable.

3.1. Energy efficiency analysis

According to the paper drying process simulation model, when the steam temperature in the cylinder is higher, the temperature and evaporation rate of the paper are higher, and the energy consumption of the cylinder is greater. When the temperature of the hot air is higher, more energy is obtained by the paper, and the energy consumption of the air hood is higher. Therefore, the cylinder steam and air hood state have a large impact on the evaporation rate of the paper and the energy consumption in the drying process. There must be an optimal balance point at which the finished paper dryness reaches the standard and the total energy consumption is a minimum.

The paper drying process simulation model provides a tool for an energy efficiency analysis of the drying process. In this work, under the same output, different cylinder pressure, hot air temperature, and fan frequency are set separately, and 4000 sets of operating parameters are obtained through combinations. The drying process simulation model is used to solve for the key variables, paper dryness, and drying energy consumption under each group of operating parameters.

To make the different operating parameter groups comparable, only those that produce a simulated dryness of the finished paper in the range of 92–92.5% are retained. When the water vapor in the air hood reaches saturation, the air temperature is the same as the dew point temperature, and the water vapor begins to condense. Water droplets formed by condensation can cause holes in the paper or rust on the equipment. To prevent this dripping phenomenon in the air hood, the exhaust air temperature must be controlled above the dew point temperature. Because the temperature distribution in the air hood shell is not uniform, to prevent the local temperature from being lower than the dew point temperature, the exhaust air temperature must be controlled to a higher

value, thus ensuring that it is different from the dew point temperature. According to practical experience, no dripping will form in the hood when this difference is above 20 °C (Dong et al. 2020). The dew point temperature can be calculated from the moisture content of air, as shown in equations (35) and (36) (Golizadeh Akhlaghi et al. 2020):

$$T_{dp} = 99.64 + 329.64 \frac{ln(P_{va}/100)}{11.78 - ln(P_{va}/100)} \tag{35}$$

$$P_{va} = P_{tot} \cdot RH_a \tag{36}$$

where T_{dp} represents the dew point temperature (℃); P_{va} represents the saturated water vapor pressure (Pa); and RH_a represents the relative humidity of air. After excluding the unqualified parameter groups of finished paper dryness and exhaust air temperature, 115 parameter groups remained. The remaining groups were sorted according to energy cost from high to low, as shown in Fig. 11.

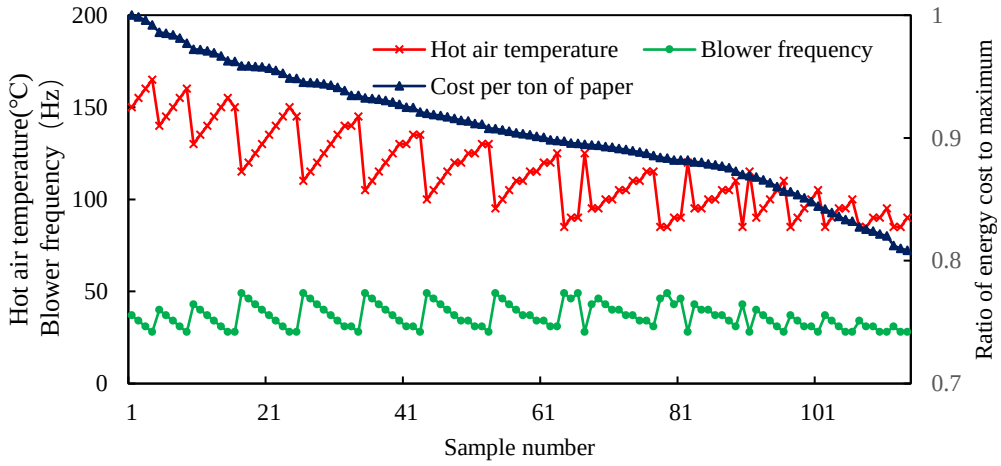

Fig. 11. Energy cost trend chart

It can be seen from Fig. 11 that under the same output, the energy costs corresponding to different groups differ by a maximum of 20%. Compared to the fan frequency, lowering the temperature of the hot air can provide more energy cost reductions. Therefore, the hot air temperature should be considered when establishing the energy system optimization model. The direct energy consumption of the paper

drying process includes the energy consumption required to evaporate the moisture and raise the temperature of the paper. In addition, there are other forms of energy consumption, namely, the heat removed by the exhaust air and the heat loss of the equipment. Therefore, the ratio of the direct energy consumption to the total energy consumption is the energy utilization efficiency of the drying process. In this work, two efficiency indicators are selected to measure the energy utilization efficiency of the drying process, namely, the cylinder and air hood thermal efficiency.

The cylinder thermal efficiency is the ratio of the heat transferred to the paper by the cylinder and the total heat released by the steam. The formula is shown in equation (37) (Qi et al. 2020).

$$\eta_c = \frac{Q_{s-p}}{\Delta H_c q_{mc}} \times 100\% \tag{37}$$

where η_c represents the cylinder thermal efficiency; Q_{s-p} represents the heat transferred from the cylinder to the paper per unit time (J/s); ΔH_c represents the change in steam enthalpy in the cylinder (J/kg); and q_{mc} is the steam flow consumed by the cylinder (kg/s).

The air hood thermal efficiency is the ratio of the heat obtained from hot air of paper to the heat consumed by the air hood, and the calculation is shown in equation (38).

$$\eta_h = \frac{\Delta H_p q_{mc} - Q_{s-p}}{\Delta H_h q_{mh}} \times 100\% \tag{38}$$

where η_h represents the air hood thermal efficiency; ΔH_p represents the enthalpy change in the paper (J/kg); $\dot{m}_p$ represents the mass flow of the paper (kg/s); ΔH_h represents the enthalpy change in the steam in the air hood (J/kg); and q_{mh} represents the steam flow consumed by the air hood (kg/s).

The cylinder and air hood thermal efficiencies can be calculated from the paper drying process simulation model, as shown in Fig. 12.

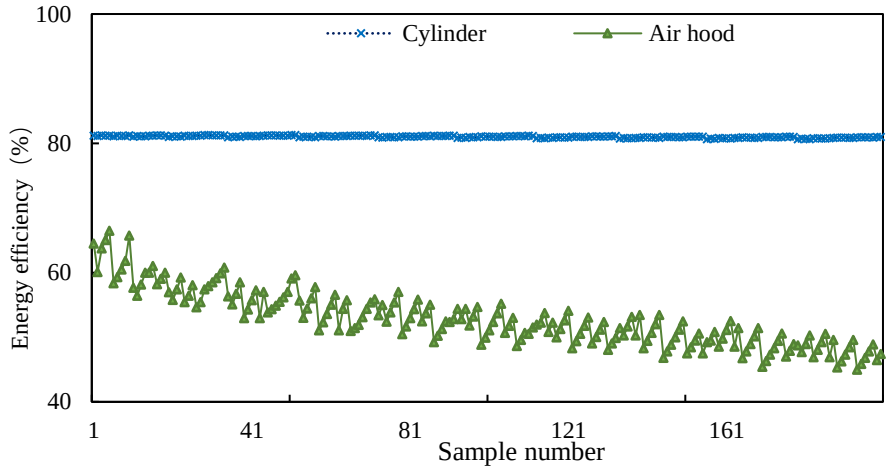

Fig. 12 Comparison of the cylinder and air hood thermal efficiency

It can be seen from Fig. 12 that the cylinder thermal efficiency is more stable and higher than that of the air hood. Through a correlation analysis, it was found that the thermal efficiency of the air hood was negatively correlated with the hot air temperature, as shown in Fig. 13.

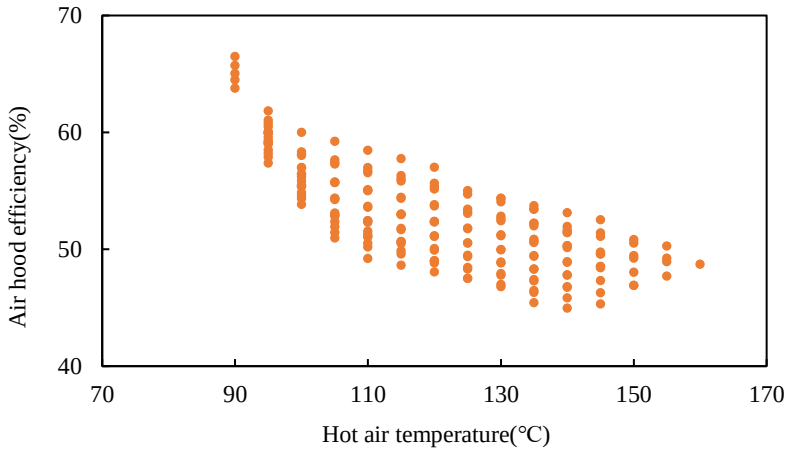

Fig. 13. Trend graph of the air hood thermal efficiency and the hot air temperature

It can be seen from Fig. 13 that the higher the hot air temperature, the lower the thermal efficiency of the air hood. This analysis shows that compared to the contact heat transfer of the cylinder, it is more difficult to absorb heat from the air hood, and a large amount of heat is removed by the exhaust air.

3.2. Modeling

3.2.1. Decision variables

Based on the results of the energy efficiency analysis, this work selects the cylinder pressure CP, the wet side hot air temperature T_w, the dry side hot air temperature T_d, and the exhaust fan frequency f_e as the decision variables for the optimization model. According to the limits of the cylinder, air hood, and exhaust fan, the feasible ranges of the decision variables are as follows:

$$P_{min} \leq CP \leq P_{max} \tag{39}$$

$$T_{1min} \leq T_w \leq T_{1max} \tag{40}$$

$$T_{2min} \leq T_d \leq T_{2max} \tag{41}$$

$$f_{min} \leq f_e \leq f_{max} \tag{42}$$

where P_{max} and P_{min} represent the upper and lower limits of the cylinder pressure, respectively (Pa); T_{1max} and T_{1min} represent the upper and lower limits of the hot air temperature of the wet side air hood, respectively (°C); T_{2max} and T_{2min} represent the upper and lower limits of the hot air temperature of the dry side air hood, respectively (°C); and f_{max} and f_{min} represent the upper and lower limits of the exhaust fan frequency, respectively (Hz).

3.2.2. Restrictions

In this work, the constraints of the energy system optimization model include the following two aspects:

(1) Dryness constraints of the finished paper. The main function of the drying process is to evaporate the moisture in the paper. When the drying process is complete, the dryness of paper should reach the standard dryness, as shown in the following equation:

$$dryness_{end} \geq dryness_{standard} \tag{43}$$

(2) Drip constraint. Based on practical experience, when the difference between

the exhaust dew point temperature and the exhaust temperature is more than 20 ℃, no dripping will occur in the air hood. For details, see section 3.1.

$$T_o \geq T_{dp} + 20 \tag{44}$$

where T_o represents the exhaust air temperature (℃).

3.2.3. Objective function

In this work, the total steam cost of the air hood and cylinder in a unit time is set as the objective function, and the calculation method is shown in equation (45):

$$Cost = (F_h + F_c) \times P_u \tag{45}$$

where $Cost$ represents the steam cost per unit time (RMB/h); P_u represents the unit price of steam (RMB/t); and F_h and F_c represent the steam flows of the air hood and cylinder (t/h).

3.2.4. Optimization algorithm

(1) Optimization algorithm based on energy efficiency analysis

Based on the results of the energy efficiency analysis, the air hood thermal efficiency is lower than that of the cylinder. Therefore, when the operating parameters are optimized, the cylinder pressure should be optimized first. If the cylinder pressure reaches the limit and the finished paper dryness still does not meet the standard, the hot air temperatures of the wet and dry sides are optimized in turn. In the optimization process, the paper drying process simulation model is used to simulate the steam flow, dew point temperature, and exhaust air temperature. If the drip constraint is not met, the exhaust fan frequency is increased until it is satisfied. The algorithm flow is shown in Fig. 15.

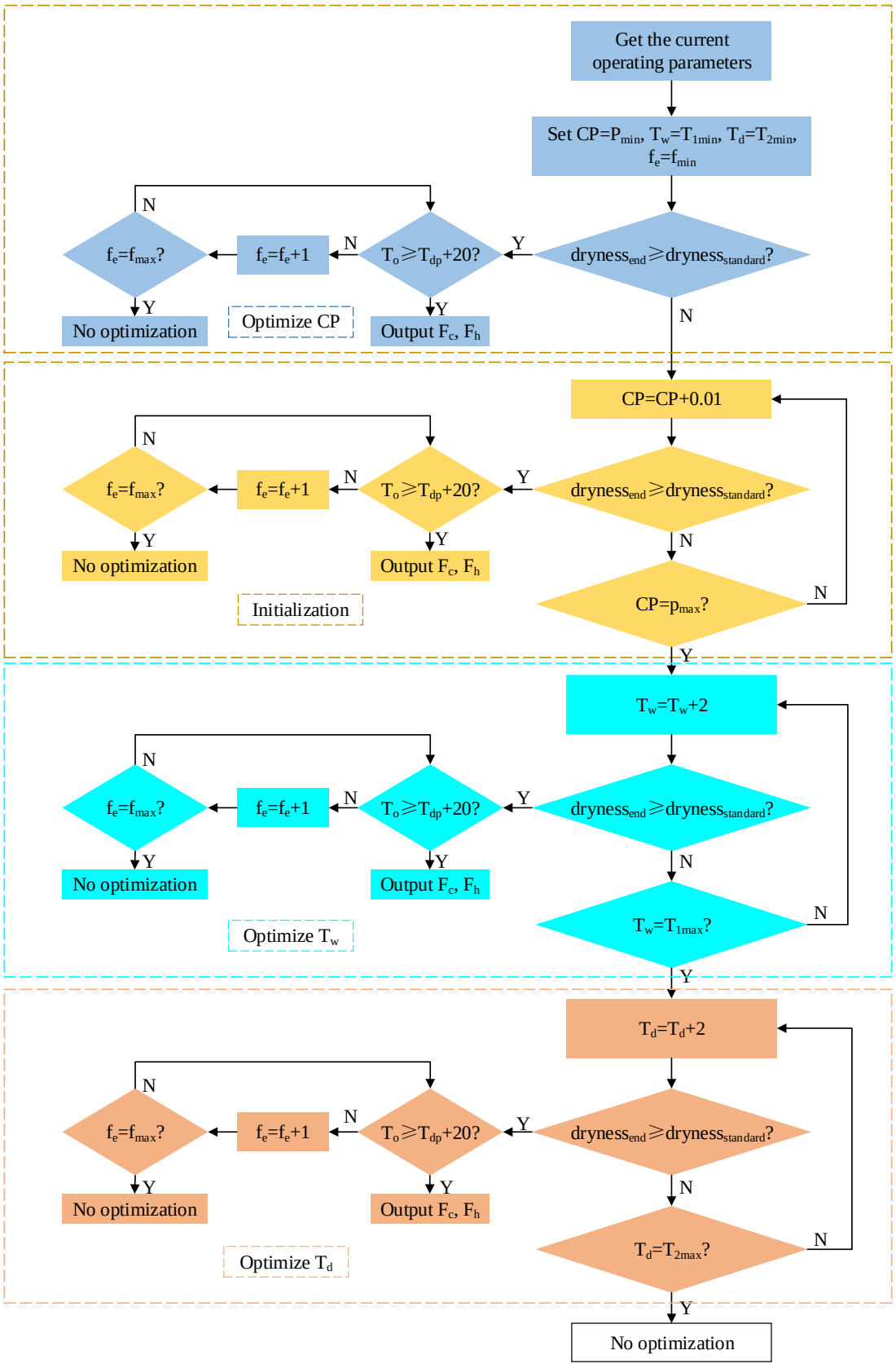

Fig. 15. Flow chart of the optimization algorithm based on energy efficiency analysis

(2) SQP algorithm

According to the simulation model of the paper drying process, there is a nonlinear characteristic between the objective function and the decision variable. Therefore, this optimization problem is a nonlinear optimization problem. SQP is currently recognized as one of the most effective algorithms for solving constrained nonlinear optimization problems. It transforms nonlinear optimization problems with constraints into a series of relatively simple quadratic programming problems for solving (Chao et al. 2008). Therefore, this work uses the SQP algorithm to solve the optimization model, as a comparison with the optimization algorithm designed based on energy efficiency analysis. The SQP algorithm description is placed in Appendix E.

3.3. Model verification

In this work, the optimization algorithm based on energy efficiency (EE) analysis and SQP algorithm are respectively used to optimize 80 groups of actual samples. Fig. 16 (a) is the change after optimization of *CP*, Fig. 16 (b) shows the change after optimization of T_w, Fig. 16 (c) illustrates the change after optimization of T_d, Fig. 16 (d) exhibits the change after optimization of f_e, Fig. 16 (e) displays the change after optimization of F_c, Fig. 16 (f) demonstrates the change after optimization of F_h, and Fig. 16 (g) is the change after optimization of *Cost*. In the energy efficiency analysis, the energy efficiency of the cylinder system is higher than that of the air hood system. Therefore, the *CP* increases after optimization while the T_w and T_d decreases, which is reflected in the solution results of the two algorithms. It is worth noting that the optimization range of T_w is far greater than that of T_d. In actual production, operators tend to take the wet side air hood as the main part, so they tend to set the hot air temperature very high, thus causing a huge waste of energy. There is no significant change before and after the optimization of f_e, because the evaporation rate does not change before and after the optimization, which is determined by the type of paper and the production speed. In addition, the optimization results of SQP algorithm on most samples are the same as those based on energy efficiency analysis, but different on a few samples. SQP algorithm performs slightly worse on these samples, which may be related to the value of the algorithm's hyperparameters. In this work, when SQP

algorithm is used, default parameters are adopted, and no separate parameter adjustment is made for different samples. However, when the interference is different, the performance of the algorithm is likely to deteriorate. After optimization, the optimization algorithm based on energy efficiency analysis and the SQP algorithm reduced F_h by 29.37% and 29.19% on average, F_c increased by 6.33% and 6.29% on average, and cost decreased by 8.71% and 8.66% on average. In summary, the optimization results of the two algorithms tend to increase *CP* and decrease hot air temperature, which is consistent with the results of energy efficiency analysis.

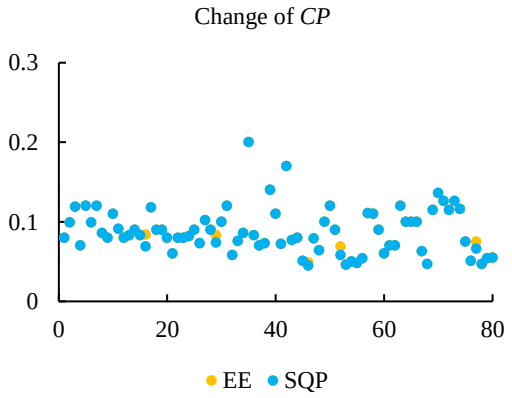

(a) The change after optimization of *CP*

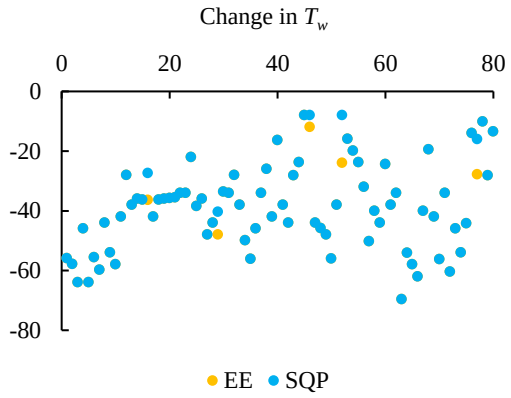

(b) The change after optimization of T_w

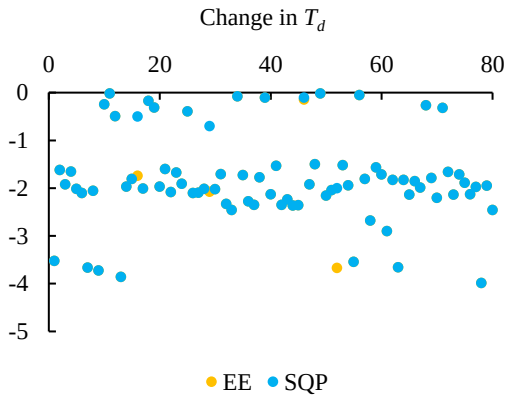

(c) The change after optimization of T_d

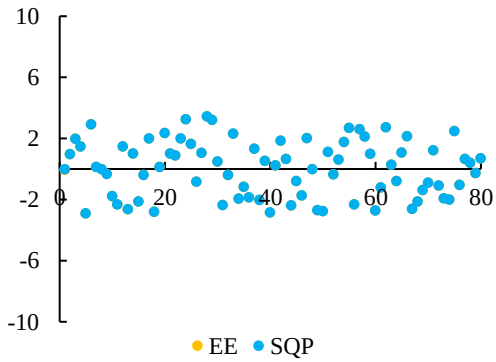

(d) The change after optimization of f_e

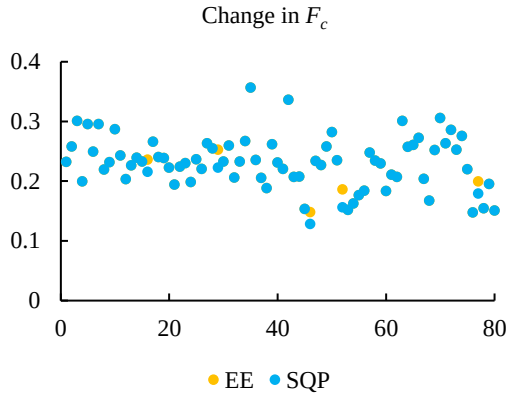

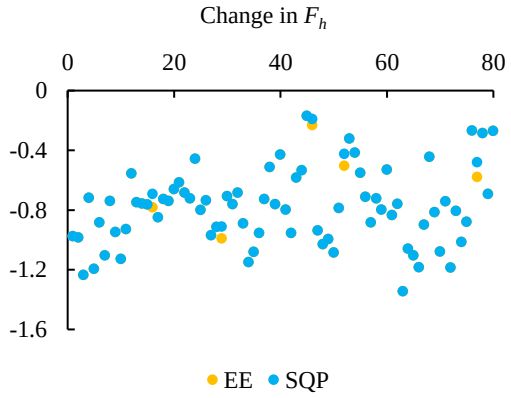

(e) The change after optimization of F_c (f) The change after optimization of F_h

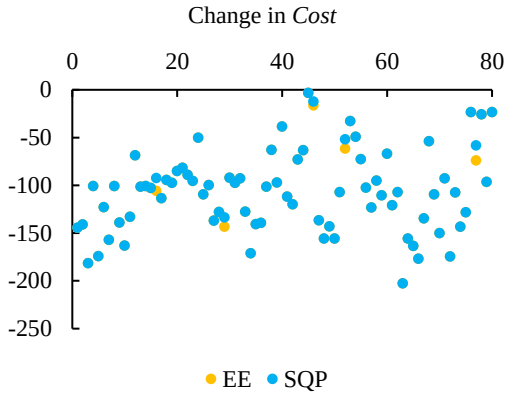

(g) The change after optimization of *Cost*

Fig. 16 Validation of energy system optimization model

4. Conclusions

This work proposes an energy system optimization model based on the simulation of key process variables in the drying process of tissue paper. The paper drying process simulation model includes three sub-models: the air hood, paper drying, and energy consumption models, which systematically consider the relationships between the environment, cylinder, air hood, and paper. The verification results show that the *MAPE* of the paper drying process simulation model for all variables is within 5%, and the *MAPE* of the evaporation rate simulation is only 1.23%. Compared with the previous model, the optimization model for the energy system proposed in this work can simultaneously optimize the cylinder pressure, hot air temperature, and exhaust fan frequency. The comprehensive consideration of the energy system makes this

optimization model more applicable. The optimization algorithm based on energy efficiency analysis and SQP algorithm are respectively used to solve the actual production samples, the results show that the model can reduce the steam cost by 8.71% for the paper mill. The models proposed in this work will serve as a reference for the modeling and optimization of multi-cylinder paper machines and provide ideas for the high quality and sustainable development of the papermaking industry.

Acknowledgements

This work was supported by the Departmental General Research Funds of the Department of Industrial and Systems Engineering, Hong Kong Polytechnic University, entitled "Green Manufacturing and Better Sustainability for Papermaking Industry: Decision-Making and Optimization in Life Cycle Perspective" (G-UAFT), Postdoctoral Fellowships Scheme, entitled "Research on Advanced Control Integration Framework for Greenhouse Gas Emission Reduction in Papermaking Wastewater Treatment Process" (G-YW4Y), and National Key R&D Program of China (2020YFE0201400).

Appendix

A. Paper machine parameter list

In this work, the paper machine parameters are a part of the model input. The paper machine parameters include two parts: the geometric parameters of the paper machine and the initial state parameters of the paper, such as the initial dryness and paper temperature after pressing. The details are shown in Table A.

Table A Paper machine parameter list

parameter name (unit)	value	parameter name (unit)	value
Cylinder diameter (m)	3.66	Number of nozzles on the dry side air hood	6611
Paper width (m)	3.4	Number of nozzles on the wet side air hood	7212

Length of *ab* section drying zone (m)	1.821	Distance between nozzle and paper (m)	0.02
Length of *bc* section drying zone (m)	3.226	Nozzle diameter (m)	0.06
Length of *cd* section drying zone	3.354	Nozzle opening rate	0.0156
Length of *de* section drying zone (m)	1.278	Longest distance between nozzle and exhaust hole (m)	0.085
Adding amount of spray liquid (kg/t)	5	Temperature of spray liquid on cylinder surface (℃)	50
Paper temperature before pressing (℃)	35	Initial dryness of paper	0.45
Paper temperature after pressing (℃)	80	Standard dryness of the finished paper	0.93

B. Historical operating data of the paper machine

In this work, the historical operating data of a paper machine are used to determine the uncertain parameters and verify the accuracy of the simulation. The data are obtained from the paper machine for four months, and the collection frequency is one data point per minute. To match the operating parameters with the quality results of the finished paper, a data preprocessing method is used to calculate the average value of the data within half an hour before the roll change. The processed data are shown in Fig. B.1 and Fig. B.2.

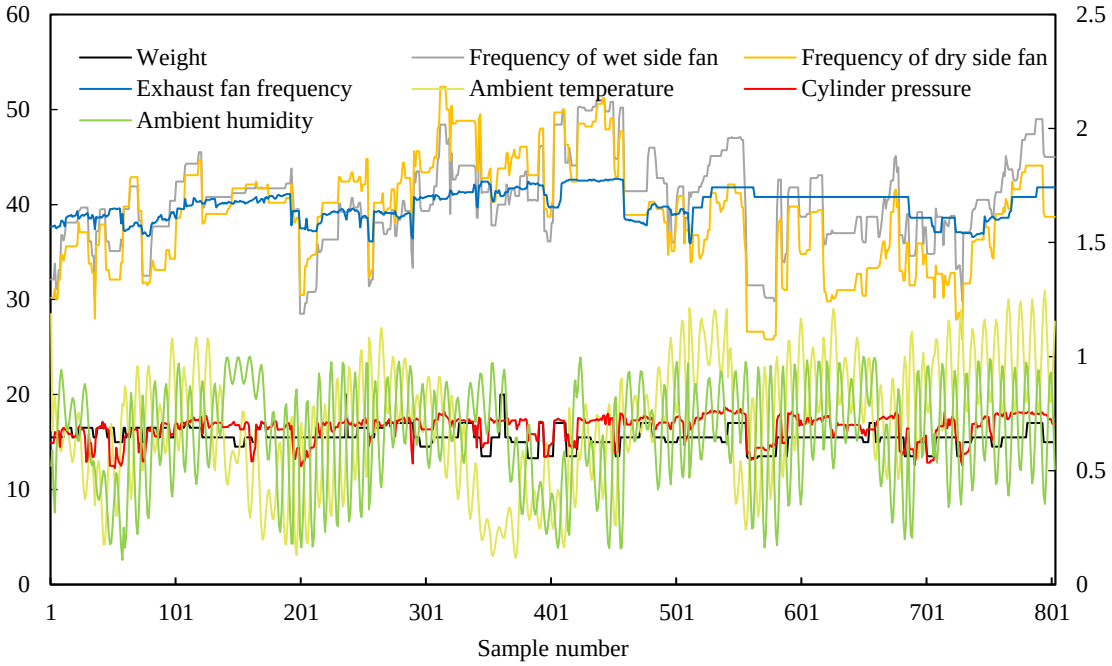

Fig. B.1. Historical operating data of the paper machine

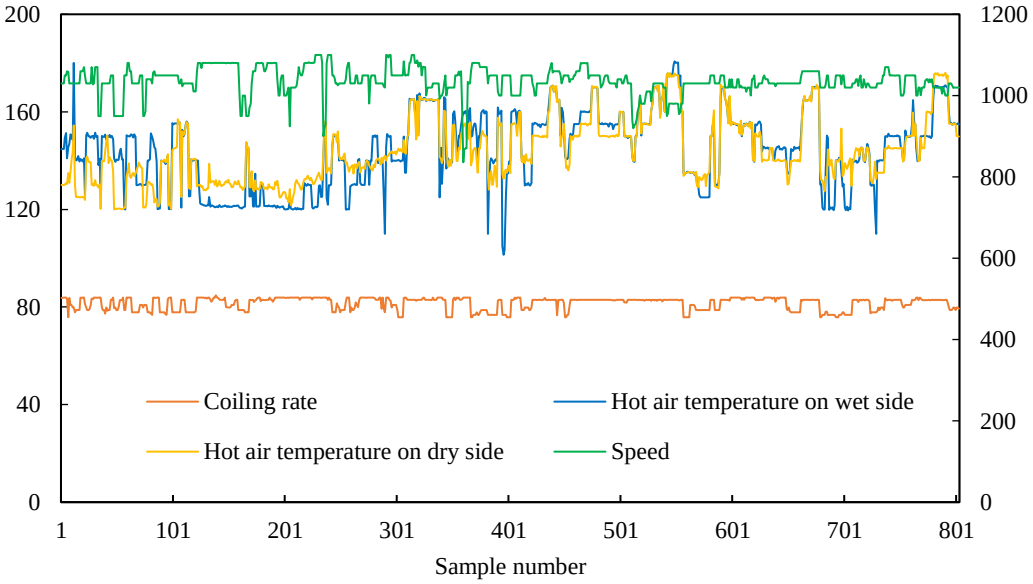

Fig. B.2. Historical operating data of the paper machine

C. Transmission information of main parameters in the model

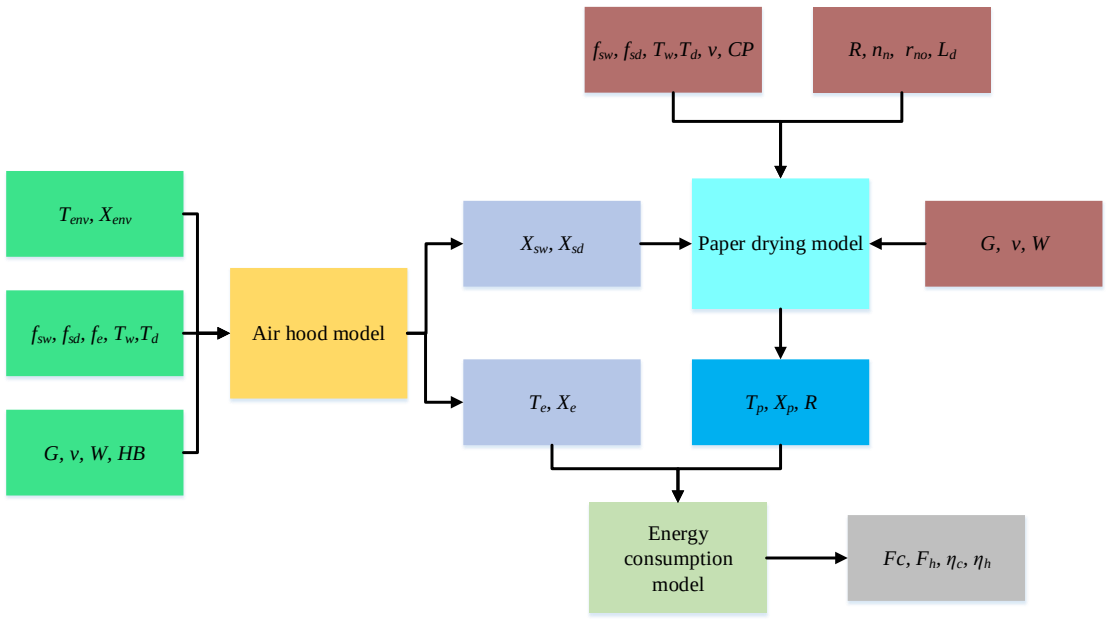

Fig. C. Parameters transfer flowchart

In Fig. D, T_{env} represents the ambient temperature, X_{env} represents the ambient humidity, f_{sw} and f_{sd} represent the wet and dry side blower frequency, T_w and T_d represent the wet and dry side hot air temperatures, f_e represents the exhaust fan frequency, v represents production speed, CP represents cylinder pressure, W represents the page width, G represents the absolute dry weight of paper, HB represents the balance rate, X_{sw} and X_{sd} represent the humidity of the wet side and dry side hot air, T_e represents the exhaust air temperature, X_e represents the exhaust air humidity, r_{no} represents the nozzle opening rate, n_n represents the nozzle number, R represents the nozzle diameter, L_d represents the length of the drying zone, T_p represents the temperature of the paper, X_p represents the humidity of the paper, F_c represents the steam flow of the cylinder, F_h represents the steam flow of the air hood, η_h represents the efficiency of the hood, η_c represents the efficiency of the cylinder.

D. Adjustment of the uncertain model parameters

Before determining the maximum number of iterations n_{iter}, assumptions are first made about the three parameters h_{s-p}, $\sum A_{ci}h_{ci}$, and $\sum A_{hi}h_{hi}$, and then the model input data are substituted into the air hood model to solve the temperature and

humidity of each key point in the pipeline during the stable operation of the paper machine. The effects under different iterations are shown in Fig. C. It can be seen that the hot air humidity, exhaust air temperature, and humidity reached stability after 40 iterations. Therefore, the maximum number of iterations n_{iter} was set to 40.

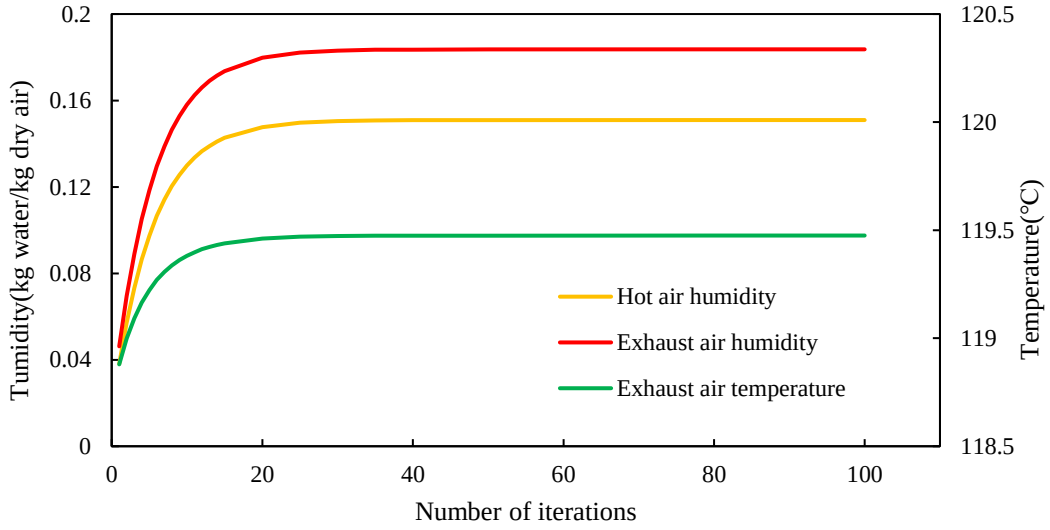

Fig. D. Effects of different iterations

In this study, 80% of the processed data is used for the adjustment of the uncertain parameters. The value of h_{s-p} is determined based on a comparison of the simulated and actual values of the evaporation rate; the value of $\sum A_{hi}h_{hi}$ is determined based on a comparison of the simulated and actual values of the air hood energy consumption; and the value of $\sum A_{ci}h_{ci}$ is determined based on a comparison of the simulated and actual values of the cylinder energy consumption. The adjustment results are listed in Table D.

Table C Parameter adjustment results

Parameter name(unit)	Value
h_{s-p} (W/(m^2·°C))	1000
$\sum A_{ci}h_{ci}$ (W/°C)	3550
$\sum A_{hi}h_{hi}$ (W/°C)	2400

E. SQP algorithm description

SQP is used to solve nonlinear problems, and its main calculation steps are as follows(Diveev et al. 2012; Chao et al. 2008):

(1) The second-order Taylor formula is used to expand the original objective function at each iteration point X^k:

$$f(X) \approx f(X^k) + (X - X^k)^T \nabla f(X^k) + \frac{1}{2}(X - X^k)^T H^k (X - X^k) \quad (1)$$

where, $\nabla f(X^k)$ represents the Jacobi matrix of the objective function at X^k, and H^k represents the Hessian matrix of the objective function at X^k. n this step, the solution of the original problem is approximately transformed into the solution of the quadratic programming (QP) problem as shown in equation (1).

(2) Take the derivative of equation (1) and set $X = X^{k+1}$ to obtain the following equation:

$$X^{k+1} \approx X^k + (H^k)^{-1}[\nabla f(X^{k+1}) - \nabla f(X^k)] = X^k + S^k \quad (2)$$

equation (2) is the iterative form of finding the optimal solution X^*, where S^k represents the iteration direction. Therefore, the solution of the above QP problem is converted to the solution of S^k. This method of solving QP problems is called Newton's method.

(3) In actual iteration, to make the iteration of each step reasonable, it is necessary to determine the iteration step length of each step α^k. In research, the backtracking line search algorithm is usually used to calculate α^k.

(4) It can be seen from equation (2) that in addition to calculating the gradient, Newton's method also needs to calculate H^k and its inverse matrix. The entire iterative process requires hardware to provide extremely powerful computing power and storage power as support. When H^k is a non-positive definite matrix, it will cause the iterative process to fail to converge, and Newton's method is completely invalid. To overcome the above two shortcomings, the quasi-Newton method was proposed, which uses a formula called BFGS to construct the H^k matrix of each iteration, and then solves the QP problem in

each iteration, as shown in equation (3):

$$H^{k+1} = H^k + \frac{1}{[\Delta X^k]^T \Delta q^k}\{\Delta X^k[\Delta X^k]^T + \frac{\Delta X^k[\Delta X^k]^T[\Delta q^k]^T H^k \Delta q^k}{[\Delta X^k]^T \Delta q^k} - H^k \Delta q^k[\Delta q^k]^T - \Delta X^k[\Delta q^k]^T H^k\} \quad (3)$$

where, the solution method of ΔX^k and Δq^k is as follows:

$$\Delta X_k = X^{k+1} - X^k \quad (4)$$

$$\Delta q^k = \nabla f(X^{k+1}) - \nabla f(X^k) \quad (5)$$

References

Chao, M., Wang, Z., Liang, Y. and Hu, Q. (2008). Quadratically constraint quadratical algorithm model for nonlinear minimax problems. *APPL MATH COMPUT* 205:247-262.

Chen, Y., He, L., Li, J. and Zhang, S. (2018). Multi-criteria design of shale-gas-water supply chains and production systems towards optimal life cycle economics and greenhouse gas emissions under uncertainty. *Comput Chem Eng* 109:216-235.

Chen, X., Li, J., Liu, H., Yin, Y., Hong, M. and Zeng, Z. (2016). Energy system diagnosis of paper-drying process, Part 1: Energy performance assessment. *Dry Technol* 34:930-943.

Chen, X., Man, Y., Zheng, Q., Hu, Y., Li, J. and Hong, M. (2019). Industrial verification of energy saving for the single-tier cylinder based paper drying process. *Energy* 170:261-272.

Diveev, A. I., Konyrbaev, N. B. and Sofronova, E. A. (2017). Method of Binary Analytic Programming to Look for Optimal Mathematical Expression. *Procedia computer science* 103:597-604.

Erkkila, A., Leppanen, T. and Hamalainen, J. (2015). Empirical plasticity models applied for paper sheets having different anisotropy and dry solids content levels (vol 50, pg 2151, 2013). *Int J Solids Struct* 69-70:569.

Di Marco, P., Frigo, S., Gabbrielli, R. and Pecchia, S. (2016). Mathematical modelling and energy performance assessment of air impingement drying systems for the

production of tissue paper. *Energy* 114:201-213.

Dong, J., Wu, L., Liu, X., Li, Z., Gao, Y., Zhang, Y. and Yang, Q. (2020). Estimation of daily dew point temperature by using bat algorithm optimization based extreme learning machine. *Appl Therm Eng* 165:114569.

Du, P., Wang, J., Guo, Z. and Yang, W. (2017). Research and application of a novel hybrid forecasting system based on multi-objective optimization for wind speed forecasting. *Energ Convers Manage* 150:90-107.

Fuentes, A., Ploteau, J. P. and Glouannec, P. (2015). Predictive control with multiobjective optimization: Application to a sludge drying operation. *Comput Chem Eng* 78:70-78.

Geng, Z., Gao, H., Wang, Y., Han, Y. and Zhu, Q. (2017). Energy saving analysis and management modeling based on index decomposition analysis integrated energy saving potential method: Application to complex chemical processes. *Energ Convers Manage* 145:41-52.

Ghodbanan, S., Alizadeh, R. and Shafiei, S. (2015). Steady-State Modeling of Multi-Cylinder Dryers in a Corrugating Paper Machine. *Dry Technol* 33:1474-1490.

Ghodbanan, S., Alizadeh, R. and Shafiei, S. (2017). OPTIMIZATION FOR ENERGY CONSUMPTION IN DRYING SECTION OF FLUTING PAPER MACHINE. *Therm Sci* 21:1419-1429.

Golizadeh Akhlaghi, Y., Badiei, A., Zhao, X., Aslansefat, K., Xiao, X., Shittu, S. and Ma, X. (2020). A constraint multi-objective evolutionary optimization of a state-of-the-art dew point cooler using digital twins. *Energ Convers Manage* 211:112772.

Gonor, A. L. (2002). High-pressure vaporization and boiling of condensed material: A generalized Clausius-Clapeyron equation, in *AIP CONFERENCE PROCEEDINGS*, M. D. Furnish, N. N. Thadhani and Y. Horie, eds., 63-66.

Grimm, A., Etula, J., Salh, R., Kalen, G., Segerstrom, M., Brucher, J., Soderberg, C., Soukup, D., Pfeifer, C. and Larsson, S. H. (2019). Slagging and fouling characteristics during co-combustion of Scots pine bark with low-temperature dried pulp and paper mill chemical sludge. *Fuel Process Technol* 193:282-294.

Heikkilä, P. and Milosavljevic, N. (2003). Influence of Impingement Temperature and

Nozzle Geometry on Heat Transfer-Experimental and Theoretical Analysis. *Dry Technol* 21:1957-1968.

Hu, Y., Li, J., Hong, M., Ren, J., Lin, R., Liu, Y., Liu, M. and Man, Y. (2019). Short term electric load forecasting model and its verification for process industrial enterprises based on hybrid GA-PSO-BPNN algorithm—A case study of papermaking process. *Energy* 170:1215-1227.

Lin, B. and Zheng, Q. (2017). Energy efficiency evolution of China's paper industry. *J Clean Prod* 140:1105-1117.

Karalashvili, M., Marquardt, W. and Mhamdi, A. (2015). Optimal experimental design for identification of transport coefficient models in convection–diffusion equations. *Comput Chem Eng* 80:101-113.

Katsiampoura, A., Toumpanakis, D., Konsta, K., Varkaris, A. and Vassilakopoulos, T. (2018). Prediction of dysnatremias in critically ill patients based on the law of conservation of mass. Comparison of existing formulae. *Plos One* 13.

Kong, L. and Liu, H. (2012). A Static Energy Model of Conventional Paper Drying for Multicylinder Paper Machines. *Dry Technol* 30:276-296.

Li, Y., Liu, H., Li, J. and Tao, J. (2011). Process Parameters Optimization for Energy Saving in Paper Machine Dryer Section. *Dry Technol* 29:910-917.

Lu, T. and Shen, S. Q. (2007). Numerical and experimental investigation of paper drying: Heat and mass transfer with phase change in porous media. *Appl Therm Eng* 27:1248-1258.

Man, Y., Han, Y., Li, J. and Hong, M. (2019a). Review of energy consumption research for papermaking industry based on life cycle analysis. *Chinese J Chem Eng* 27:1543-1553.

Man, Y., Han, Y., Li, J. and Hong, M. (2019b). Review of energy consumption research for papermaking industry based on life cycle analysis. *Chinese J Chem Eng* 27:1543-1553.

Man, Y., Hong, M., Li, J., Yang, S., Qian, Y. and Liu, H. (2017). Paper mills integrated gasification combined cycle process with high energy efficiency for cleaner production. *J Clean Prod* 156:244-252.

Nilsson, L. (2004). Heat and mass transfer in multicylinder drying: Part I. Analysis of machine data. *Chemical Engineering and Processing: Process Intensification* 43:1547-1553.

Nouri, M., Rahpaima, G., Nejad, M. M. and Imani, M. (2018). Computational simulation of CO2 capture process in a fluidized-bed reactor. *Comput Chem Eng* 108:1-10.

Ottosson, A., Nilsson, L. and Berghel, J. (2017). A mathematical model of heat and mass transfer in Yankee drying of tissue. *Dry Technol* 35:323-334.

Ortega, A. and Juan Rosales, J. (2018). Newton's law of cooling with fractional conformable derivative. *Rev Mex Fis* 64:172-175.

Peng, L., Zeng, X., Wang, Y. and Hong, G. (2015). Analysis of energy efficiency and carbon dioxide reduction in the Chinese pulp and paper industry. *Energ Policy* 80:65-75.

Qi, C., Li, K., Li, C., Shang, B. and Yan, Y. (2020). Experimental study on thermal efficiency improvement using nanofluids in heat sink with heated circular cylinder. *Int Commun Heat Mass* 114:104589.

Soto-Meca, A., Serna, J. and Velasco, F. J. S. (2016). Heat and mass transfer enhancement in a double diffusive mixed convection lid cavity under pulsating flow. *Comput Chem Eng* 94:128-140.

Welty, J. R., Wicks, C. E. and Wilson, R. E. (1976). Fundamentals of momentum, heat, and mass transfer, 2nd edition, 789.